ORIGINAL RESEARCH

Composite Microgels Loaded with Doxorubicin-Conjugated Amine-Functionalized Zinc Ferrite Nanoparticles for Stimuli-Responsive Sustained Drug Release

Shirisha Bellala[1],*, Karthika Viswanathan[2],*, Ujwala Guntakanti[3], Anitha Kowthalam[1], Sung Soo Han[4], Madhusudana Rao Kummara[4], Sreekanth Reddy Obireddy [iD][1,5], Wing-Fu Lai [iD][5–7]

[1]Department of Chemistry, Sri Krishnadevaraya University, Anantapur, Andhra Pradesh, 515003, India; [2]Department of Nanoscience and Technology, Alagappa University, Karaikudi, Tamil Nadu, 630 003, India; [3]Department of Chemistry, G. Pulla Reddy Engineering College, Kurnool, Andhra Pradesh, 518 007, India; [4]School of Chemical Engineering, Yeungnam University, Gyeongsan, 38541, Republic of Korea; [5]Department of Urology, Zhejiang Provincial People's Hospital, Affiliated People's Hospital, Hangzhou Medical College, Zhejiang, 310014, China; [6]School of Food Science and Nutrition, University of Leeds, Leeds, LS2 9JT, UK; [7]Department of Applied Biology and Chemical Technology, Hong Kong Polytechnic University, Hong Kong Special Administrative Region, China

*These authors contributed equally to this work

Correspondence: Wing-Fu Lai, Email rori0610@graduate.hku.hk; Sreekanth Reddy Obireddy, Email sreekanthchem7@gmail.com

Purpose: The purpose of this study is to address the need for efficient drug delivery with high drug encapsulation efficiency and sustained drug release. We aim to create nanoparticle-loaded microgels for potential applications in treatment development.

Methods: We adopted the process of ionic gelation to generate microgels from sodium alginate and carboxymethyl cellulose. These microgels were loaded with doxorubicin-conjugated amine-functionalized zinc ferrite nanoparticles (AZnFe-NPs). The systems were characterized using various techniques. Toxicity was evaluated in MCF-7 cells. In vitro release studies were conducted at different pH levels at 37 °C, with the drug release kinetics being analyzed using various models.

Results: The drug encapsulation efficiency of the created carriers was as high as 70%. The nanoparticle-loaded microgels exhibited pH-responsive behavior and sustained drug release. Drug release from them was mediated via a non-Fickian type of diffusion.

Conclusion: Given their high drug encapsulation efficiency, sustained drug release and pH-responsiveness, our nanoparticle-loaded microgels show promise as smart carriers for future treatment applications. Further development and research can significantly benefit the field of drug delivery and treatment development.

Keywords: sodium alginate, carboxymethyl cellulose, doxorubicin, zinc ferrite nanoparticles, microgels

Introduction

Nanoformulations based on polymers, proteins, lipids, metals, or inorganic materials have been extensively developed over the years.[1–3] These formulations exhibit good bioavailability, targeting capacity, and the ability to enhance drug stability,[3] demonstrating the promising future of nanomedicine in mediating detection and treatment of a wide range of disorders.[4–7] Among different types of nanoparticles (NPs), metallic nanoparticles generally exhibit high biocompatibility, low toxicity, and high structural stability.[8] Magnetite NPs (MNPs) are the only metallic nanoparticles that have received approval from the US Food and Drug Administration (FDA) for use in biomedical applications.[9] More recently, Adilakshmi and coworkers examined the anti-cancer effect of doxorubicin (DOX)-encapsulated amine-functionalized magnetic nanoparticle nanocomposites on MCF-7 cells.[1] They found that the developed nanocomposites enabled reactive oxygen species (ROS) generation and displayed excellent anti-cancer activity.

In recent years, much interest has been devoted to the study of zinc oxide NPs for light-responsive ROS generation. Chemical modifications (such as doping with other metals, functionalization of NPs, and polymer functionalization) can improve the photocatalytic activity and ROS-generating capacity of zinc oxide (ZnO) NPs.[10] ZnO NPs have been classified by US FDA as a GRAS (generally regarded as safe) material.[11,12] Along with their ease of fabrication, ZnO NPs have been reported for a wide variety of medical applications, including antibacterial therapy, wound treatment and bioimaging.[13–16] Modified ZnO NPs showed enhanced antibacterial and anticancer action due to increased ROS generation efficiency.[10] This is demonstrated by the case of curcumin-encapsulated ZnO NP-containing nanocomposites, which demonstrated effective anticancer effects on rhabdomyosarcoma cells.[17]

Since the turn of the last century, biodegradable polymers have been the subject of intensive drug delivery research as well, partly because of their good biodegradability, good biocompatibility, low toxicity and high drug loading efficiency.[18–21] Sodium alginate (SA) is an anionic polysaccharide being nontoxic and hydrophilic. SA can interact with multivalent cations (such as Ca^{2+}, Mg^{2+}, and Ba^{2+}) to form 3D network hydrogel beads.[22–24] On the other hand, sodium carboxymethyl cellulose (CMC), an anionic cellulose derivative, can be created by adding carboxymethyl groups to cellulose. It can also swell and produce hydrogel beads when exposed to multivalent cations.[25,26] Both SA and CMC are pH-sensitive polymers widely used in various biomedical applications in the form of hydrogels.[27–29] Despite this, pure hydrogels have insufficient mechanical strength because of their fragile networks after maximal swelling.[30] To address this problem, hydrogels have been incorporated with inorganic nanoparticles [such as clay and metal oxides (eg, iron oxide, CuO, and ZnO)].[31–35] Not only can this enhance the mechanical strength and encapsulation efficiency of the hydrogel,[36,37] but the drug release sustainability can also be enhanced.[20]

In this study, the gelation technique has been used to create nanoparticle-embedded microgels for drug delivery. The ionotropic gelation technique has several advantages over alternative formulation techniques.[38,39] Major advantages of this procedure are that it is quick, simple, easy-to-operate and cost-effective. In comparison to chemical crosslinking, the reversibility of physical cross-linking via electrostatic interaction permits the avoidance of potential toxicity and other unfavourable effects for biomedical applications. The technique can be optimized based on polymer-drug interactions, leading to increased encapsulation efficiency.[40,41] In the present work, we have developed amine-functionalized zinc ferrite NPs (AZnFe-NPs) coupled with DOX and embedded into SA/CMC matrices for drug delivery. The developed composite microgels have been analyzed using different characterization techniques. The impact of NPs on swelling and release studies has also been investigated.

Materials and Methods
Materials
All chemicals used in this work were of analytical grade and were utilized without prior purification. CMC, $CaCl_2$, and diethylenetriamine were obtained from Merck (Mumbai, India). SA, sodium acetate, iron (III) chloride hexahydrate, zinc chloride, and glycerol were obtained from SD Fine Chemicals (Mumbai, India). DOX was a gift sample from Aurobindo Pharma Ltd., Telangana, India.

Synthesis of Amine-Functionalized Zinc Ferrite Nanoparticles
To synthesize AZnFe-NPs, diethylenetriamine, sodium acetate, iron (III) chloride hexahydrate, and zinc chloride were dissolved in glycerol in a stoichiometric ratio under vigorous stirring. After that, the solution was placed inside an autoclave and kept at 180 °C for 6 h. The generated AZnFe-NPs were washed with DI water and ethanol multiple times, dried at 40 °C, and stored for later use in airtight containers.

Synthesis of DOX-Conjugated AZnFe-NPs and Microgels
To synthesize DOX-conjugated AZnFe-NPs (DOX-AZnFe-NPs), the procedure outlined in our previous work was adopted with a slight modification.[35] Briefly, 10 mg of AZnFe-NPs were dispersed in deionized (DI) water and sonicated for 30 min to form a homogenous dispersion. DOX (5 mg per 5 mL of DI water) was added to the dispersion, followed by the addition of 1-ethyl-3-(3-dimethylaminopropyl)carbodiimide (EDC) and N-hydroxysuccinimide (NHS). The

reaction mixture was stirred for 24 h at 37 °C. The resultant mixture was centrifuged at 15,000 rpm for 10 min. The generated DOX-AZnFe-NPs were stored at −5 °C.

To synthesize the DOX-loaded polymeric microgels and DOX-AZnFe-NPs-loaded microgels, 200 mg each of SA and CMC was dispersed in 10 mL of DI water. After that, 200 μL of SA and 200 μL of CMC were combined and agitated to create a homogenous solution. DOX-AZnFe-NPs were added to this solution, stirred for 6 hours, and then dropped into a CaCl₂ solution to create composite microgels (SACMC-DOX-AZnFe-NPs). Similarly, SACMC-AZnFe-NPs and SACMC-DOX microgels were prepared by using the above process. AZnFe-NPs and DOX were added to the polymer solution to form SACMC-AZnFe-NPs and SACMC-DOX microgels, respectively. The obtained microgels were washed with DI water multiple times to remove free DOX, dried at room temperature, and stored in air-tight containers for subsequent use.

Materials Characterization

The FTIR spectra of DOX, AZnFe-NPs, DOX-AZnFe-NPs, SA/CMC mixture, SACMC-DOX, SACMC-AZnFe-NPs, and SACMC-AZnFe-NPs were analyzed using the Bomem MB-3000 instrument. A wide-angle X-ray scattering diffractometer (Panalytical X-ray Diffractometer, model-X'pert Pro) was used to measure the X-ray diffraction (XRD) patterns of DOX, SACMC-DOX, AZnFe-NPs, SACMC-DOX-AZnFe-NPs, and SACMC-AZnFe-NPs. Thermal analysis of DOX, AZnFe-NPs, SACMC-DOX, and SACMC-DOX-AZnFe-NPs was conducted by heating the sample from 35 to 600 °C in a nitrogen atmosphere by using a DSC-SP instrument (Rheometric Scientific, UK). Morphological features of SACMC-DOX, SACMC-AZnFe-NPs, SACMC-DOX-AZnFe-NPs, and AZnFe-NPs were characterized via scanning electron microscopy (SEM) (JOEL MODEL JSM 840A). The size of AZnFe-NPs was measured using transmission electron microscopy (TEM; JEOL JEM 2100; JEOL, Japan). The size and polydispersity index (PDI) of the AZnFe-NPs were determined by dynamic light scattering (DLS) using a Zetasizer Nano-ZS instrument (Malvern, UK).

Encapsulation Efficiency (EE)

The EE of SACMC-DOX and SACMC-DOX-AZnFe-NPs microgels was determined by following the procedures as previously described.[42] In brief, 3 mg of SACMC-DOX and SACMC-DOX-AZnFe-NPs was weighed and dispersed overnight in 5 mL of phosphate buffer at ambient conditions. After that, the mixture was ultrasonically agitated for 10 minutes and then crushed to extract DOX from the drug-loaded microgels. The amount of the extracted drug was assayed at 481 nm by using UV-visible (UV-vis) spectroscopy. The EE was determined by using the equation as previously reported.[43]

Swelling Capacity

The swelling behavior of SACMC-DOX, SACMC-AZnFe-NPs, and SACMC-DOX-AZnFe-NPs microgels was examined at different pH (6.0 and 7.4) at 37 °C by following the procedures as previously described.[44,45] The swelling degree (%SD) was calculated by using the following formula:

$$\%SD = \frac{W_w - W_d}{W_d} \times 100\%$$

where W_w and W_d designate the weight of the wet microgel and the weight of the dry microgel, respectively.

In Vitro Release Study and Its Kinetics

To determine the drug release profiles of the synthesized microgels, dialysis bags containing 5 mg of SACMC-DOX and SACMC-DOX-AZnFe-NPs microgels were submerged in 30 mL of PBS (pH 6.0 or 7.4) at 37°C and were subjected to constant stirring at 50 rpm. Two milliliters of the dissolution fluid were sampled at regular time intervals and replaced with the same volume of fresh PBS. The amount of DOX in the sampled medium was determined at 481nm by using a UV-vis spectrophotometer. The data obtained were fitted into different kinetic models (including the zeroth order model, Higuchi model, first order model, and Korsmeyer-Peppas model) in order to evaluate the drug release kinetics.[46,47]

MTT Assay

The MTT assay was performed on MCF-7 cells using a published method.[48] MCF7 cells (purchased from National Centre for Cell Science, Pune, India) were placed in a 96-well plate with the addition of 200 μL of DMEM to each well. After a 24-h incubation at 37°C in a 5% CO2 atmosphere, test samples (DOX, SACMC-DOX, SACMC-AZnFe-NPs, and SACMC-DOX-AZnFe-NPs) were introduced to each well at varying concentrations. The cells were exposed to the test samples for an additional 24 h at 37°C in a 5% carbon dioxide environment. Following this, the MTT reagent was applied to each well at a concentration of 0.5 mg/mL, and the plate was incubated at 37°C for 3 h. After removing the unreacted reagent, the violet crystals in each well were dissolved in 100 μL of DMSO, and the color intensity was measured using an ELISA reader at a wavelength of 570 nm.

Results and Discussion

Structural Characterization

AZnFe-NPs were synthesized and loaded with DOX before being embedded into the polymeric matrix to form composite microgels. Generation of amine-functionalized AZnFe-NPs (as well as the interactions between DOX and AZnFe-NPs, between DOX-conjugated AZnFe-NPs and polymeric matrix, and between AZnFe-NPs and the polymeric matrix) were analyzed by FTIR (Figure 1). The stretching vibrations of O-H/N-H, C=O, C-N, and C-O, respectively, were attributed to the absorption bands at 3328, 1732, 1288, and 1072 cm^{-1} in the spectrum of DOX. The bending vibrations of N-H, C=C,
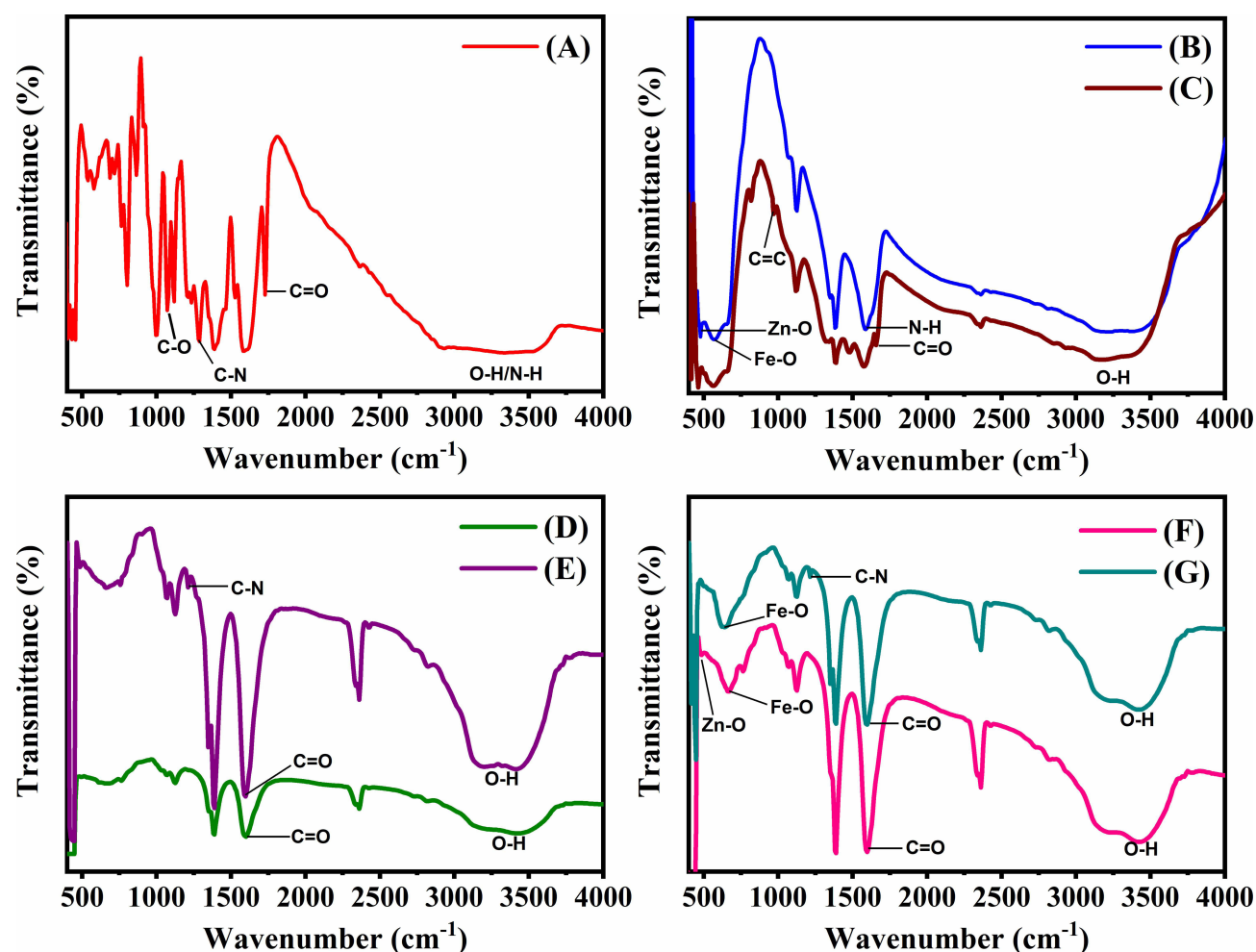

Figure 1 FTIR spectra of (**A**) DOX, (**B**) AZnFe-NPs, (**C**) DOX-AZnFe-NPs, (**D**) placebo (plain SA/CMC matrix), (**E**) SACMC-DOX, (**F**) SACMC-AZnFe-NPs, and (**G**) SACMC-DOX-AZnFe-NPs.

and C-H, respectively, were assigned to the bands at 1589, 995, and 802 cm^{-1}.[9] The Zn-O bond in the tetrahedral site and the Fe-O bond in the octahedral site of AZnFe-NPs exhibited stretching vibrations at 563 and 462 cm^{-1}, respectively, whereas the band at 1589 cm^{-1} was attributed to the N-H bending vibrations of AZnFe-NPs.[49] In the spectrum of DOX-conjugated AZnFe-NPs, similar bands of AZnFe-NPs were observed. New bands at 1656, 966, and 825 cm^{-1} (which were attributed to vibrations of C=O, C=C, and C–H, respectively, of the DOX molecule) were found. The presence of these bands confirmed that the DOX successfully conjugated with AZnFe-NPs.[50] The bands at 3435 and 1601 cm^{-1} for the plain SA/CMC mixture (which was used as a placebo in this study) were attributed to stretching vibrations of –COOH and those of O–H and C=O, respectively. In the spectrum of SACMC-DOX, the C=O stretching frequency was shifted to 1597 cm^{-1}. This indicated that DOX was effectively loaded into the polymeric matrix. In addition, two new bands, 1335 and 1214 cm^{-1}, were observed and assigned to DOX. The presence of new bands at 662, 490 and 638 cm^{-1} in the spectrum of the SACMC-AZnFe-NPs revealed that AZnFe-NPs were successfully loaded into the polymeric matrix. The spectrum of SACMC-DOX-AZnFe-NPs exhibited bands that were comparable to those found in the spectra of SACMC-DOX and SACMC-AZnFe-NPs. This confirmed the presence of DOX-conjugate AZnFe-NPs.

To find out the crystallinity and molecular dispersion of DOX and NPs in the polymeric matrix, XRD analysis was performed (Figure 2). The diffraction 2Θ peaks of free DOX revealed the good crystalline structure of DOX. On comparison, the disappearance of the crystalline 2Θ peak of DOX in microgels confirmed that DOX existed in an amorphous state after being loaded into the microgels. The XRD patterns of AZnFe-NPs showed 2Θ peaks at 30.01, 35.6, 42.98, 53.56, 57.3, and 62.7°. These peaks were attributed to the (220), (311), (400), (422), (511), and (440) planes, respectively (JCPDS No. 01–079-1150).[51] Based on the high similarity in the XRD patterns of SACMC-AZnFe-NPs and SACMC-DOX-AZnFe-NPs, the AZnFe-NPs were suggested to be successfully incorporated into the polymeric matrix.

Thermal Analysis

The crystallinity of DOX and the thermal stability of microgels were evaluated using thermal analysis (Figure 3). A distinct peak at 247.5 $^{\circ}$C was found in the differential scanning calorimetry (DSC) curve of DOX, and this was thought to be the
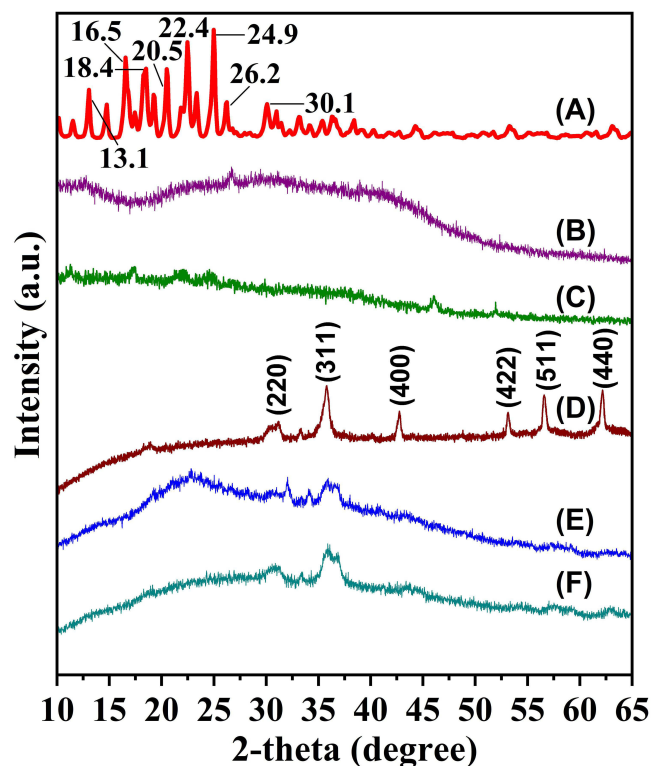
Figure 2 XRD patterns of (**A**) DOX, (**B**) placebo, (**C**) SACMC-DOX, (**D**) AZnFe-NPs, (**E**) SACMC-DOX-AZnFe-NPs, and (**F**) SACMC-AZnFe-NPs.
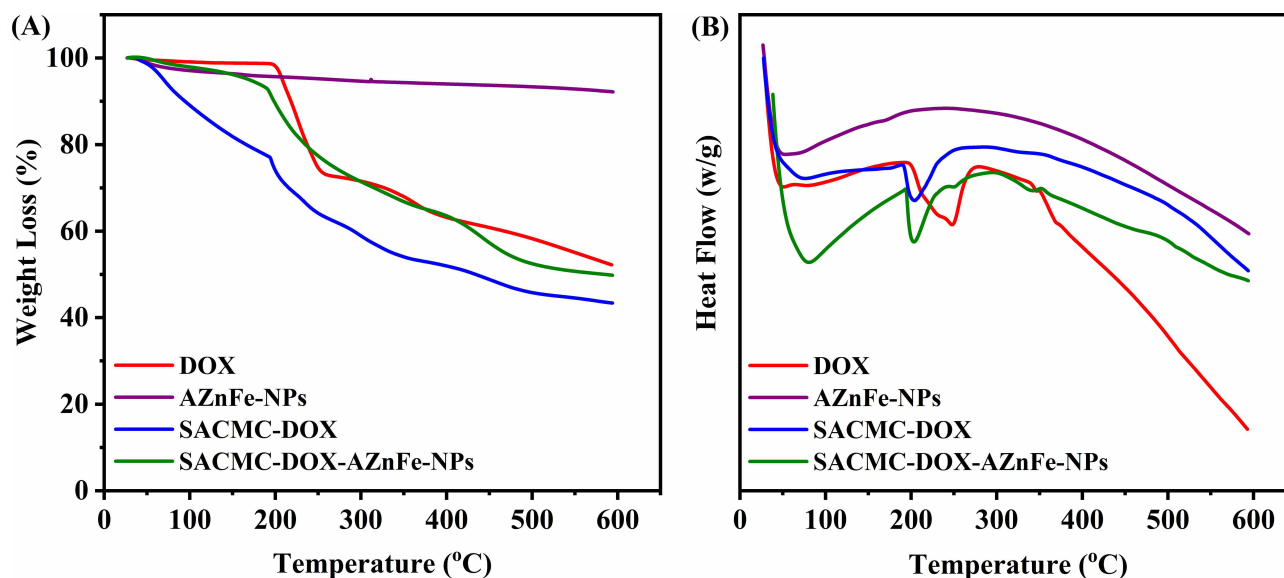
Figure 3 A) DSC and (**B**) TGA curves of DOX, AZnFe-NPs, SACMC-DOX, and SACMC-DOX-AZnFe-NPs.

melting point of the drug. The disappearance of this peak in SACMC-DOX and SACMC-DOX-AZnFe-NPs showed that the DOX was dispersed consistently throughout the microgels. The thermogravimetric analysis (TGA) curve of DOX revealed two stages of decomposition. The first stage with a 27.6% mass loss occurred between 196 and 260 °C, possibly due to the release of HCl. The second stage with a loss of 8.7% was found between 262 and 383 °C, possibly due to the loss of the initial mass of DOX.[52,53] TGA data showed that the mass of AZnFe-NPs decreased by only 7.8% from 35 to 600 °C, indicating that they experienced only mild thermal deterioration. The TGA curves of SACMC-DOX-AZnFe-NPs showed three decomposition stages. The first stage, with a weight loss of 8%, was found between 35 and 189 °C. This loss was due to the evaporation of adsorbed water molecules. The second stage, with a weight loss of 30%, was observed between 194 and 417 °C. The loss was due to the formation of sodium carbonate residue. The third stage was found between 421 and 600 °C with a weight loss of 12% due to the thermal decomposition of the polymer blend.[54] The weight loss of SACMC-DOX-AZnFe-NPs was less than that of SACMC-DOX, demonstrating that the stability was improved by the addition of AZnFe-NPs.[55] The increased thermal stability of the generated microgels was demonstrated by the TGA data.

Morphological Analysis

The morphological features of AZeFe-NPs and NPs-loaded microgels (Figure 4) play a pivotal role in determining the performance in drug delivery. The morphology of the microgels was found to be spherical in shape, exhibiting a smooth surface as depicted in images (a-d). However, upon being loaded with AZeFe-NPs, the microgels displayed a distinct transformation in morphology, featuring a rough and wrinkled surface. This morphological change suggested that the incorporation of NPs had a significant impact on the microgel structure, potentially influencing their subsequent drug release sustainability. The average size of microgels, based on the SEM images, was found to be 600–800 µm. Moreover, the synthesized amine-functionalized ZnFe-NPs exhibited a uniform size in the range of 120–150 nm, as evidenced in the TEM images (e and f). This finding was consistent with the results of our DLS analysis (Figure 4g), which estimated a mean particle size of 163 nm for AZeFe-NPs. The high dispersion nature of the synthesized NPs, as indicated by the low polydispersity index (0.295), suggested homogeneous distribution which could enhance stability and could ensure consistent drug release kinetics. The rough and wrinkled surface of NPs-loaded microgels may enhance the drug encapsulation efficiency and may also influence release kinetics as depicted in the subsequent section of this article.
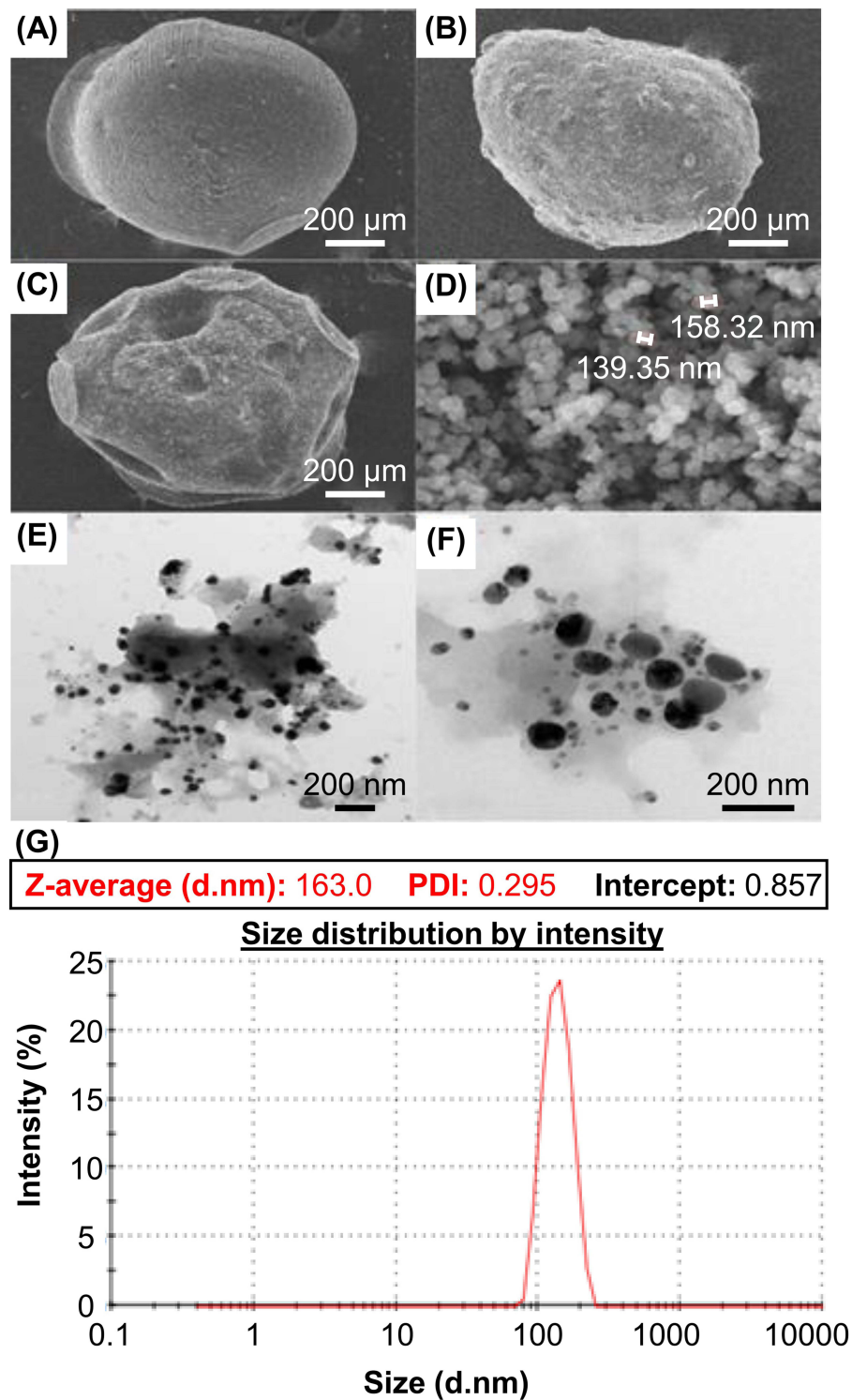
Figure 4 SEM images of (**A**) SACMC-DOX, (**B**) SACMC-AZnFe-NPs, (**C**) SACMC-DOX-AZnFe-NPs, and (**D**) AZnFe-NPs. TEM images of AZnFe-NPs (E & (**F**). The DLS graph of AZeFe-NPs (**G**).

Drug Encapsulation and Release

The EE of SACMC-DOX and SACMC-DOX-AZnFe-NPs was found to be 72.1% and 78.4%, respectively. The impact of AZnFe-NPs on DOX encapsulation was examined using microgels containing DOX-conjugated AZnFe-NPs. The presence of AZnFe-NPs increased the amount of DOX in the microgels.[56] This was attributed to the fact that DOX and

AZnFe-NPs formed an imine bond and exhibited electrostatic interactions. As a consequence of these interactions, the EE of DOX in the microgels increased.[56] A similar observation was reported by Akl and coworkers, who found that the combination of DOX with tri-sodium citrate functionalized magnetite nanoparticles results in high encapsulation efficiency due to the formation of an imine bond between DOX and NPs.[57] The swelling behavior of SACMC-DOX and SACMC-AZnFe-NPs-DOX was determined at 37 °C under different physiological conditions (pH 7.4 and pH 6.0) (Figure 5C). The generated microgels were found to swell more significantly at pH 7.4 than at pH 6.0. The difference in swelling behavior was attributed to the ionization effects on the polymeric chains of SA and CMC under acidic conditions. At pH 6.0, the ionization process led to the formation of complex networks among the polymeric chains, resulting in a reduction of the swelling nature of the polymeric network. At pH 7.4, the carboxylic groups of SA-CMC polymeric chains underwent ionization into carboxylate ions, leading to enhanced electrostatic interactions between SA and CMC chains. This phenomenon resulted in a higher degree of swelling, indicating a pH-dependent response of the polymeric microgels. The findings suggested that pH played a significant role in modulating the swelling behavior of SACMC-based microgels and this is a critical aspect for designing drug delivery systems with tailored release kinetics.[54] Furthermore, incorporation of AZnFe-NPs into the microgels contributed to a higher degree of swelling. The presence of NPs in the matrix created pores, facilitating the diffusion of the medium into the polymeric matrix. This increased swelling behavior was attributed to the porous structure formed by the NPs within the microgel matrix.[20] Our finding highlighted the interplay between the polymeric matrix, pH, and the influence of NPs in determining the swelling characteristics of the microgels. Such insights will be valuable for subsequent rational design of drug delivery systems, where controlled swelling behavior is crucial for achieving optimal drug release profiles.
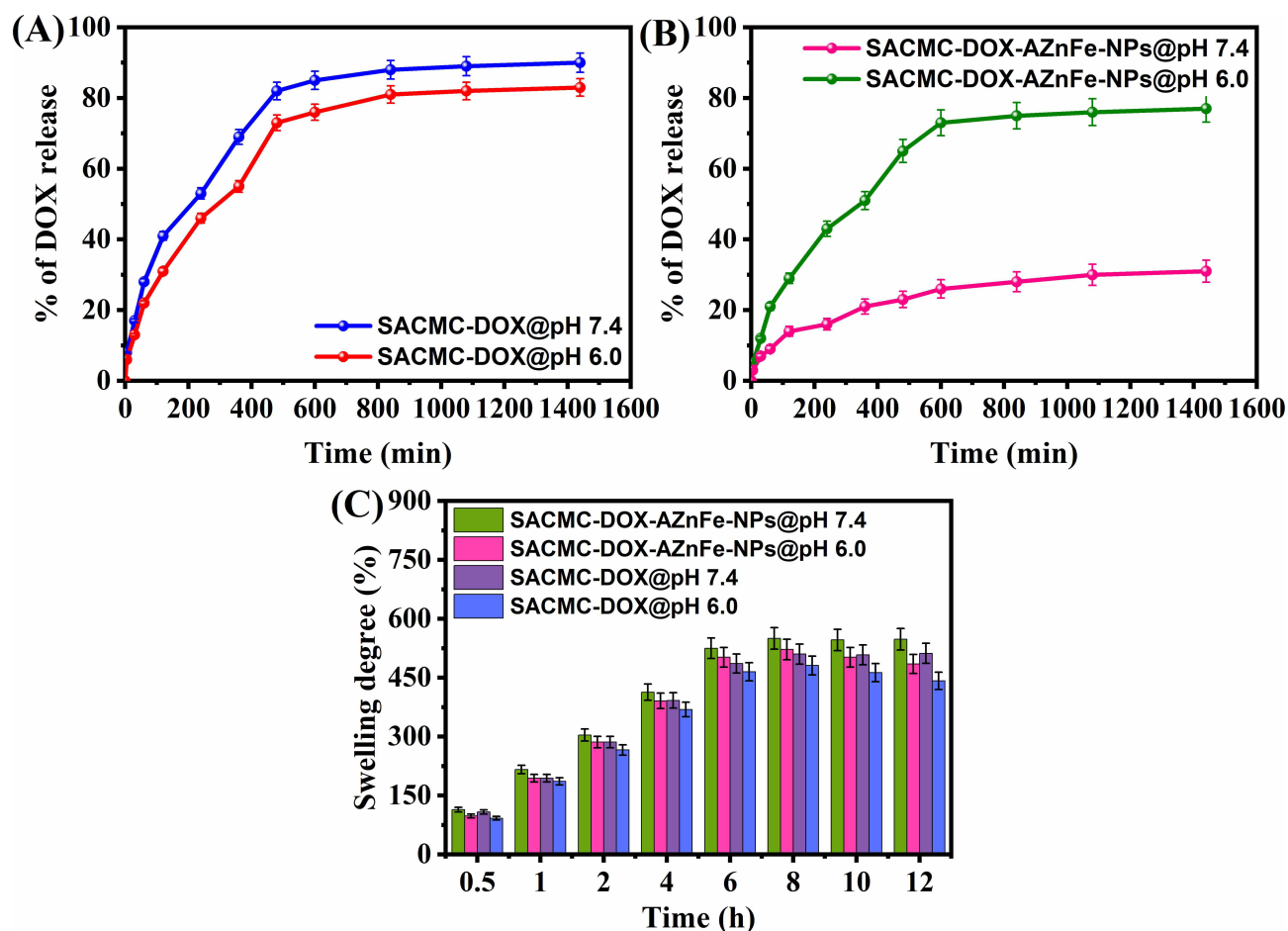
Figure 5 A) and (**B**) In vitro release profiles as well as the (**C**) swelling capacity of SACMC-DOX and SACMC-DOX-AZnFe-NPs at pH 7.4 and 6.0 at 37 °C (n = 3). Data are shown as mean ± SD.

The drug release profiles of the generated microgels were determined at pH 7.4 and 6.0 (Figure 5A). AT pH 7.4, drug release from microgels in PBS was maximal 8 h after the start of the experiment; whereas at pH 6.0, a lesser amount of DOX was released. The comparison of the drug release profiles of SACMC-DOX and SACMC-DOX-AZnFe-NPs microgels at pH 7.4 and 6.0 revealed different release mechanisms, which were thought to be dependent on the nature of the cationic ions present in the buffer media. The media at pH 6.0 was slightly acidic in nature. Hydrogen bonding in the SA/CMC polymeric matrix may lead to the formation of hydrophobic networks. The carboxyl groups of the SA/CMC polymeric matrix were not completely ionized in the acidic environment, too. These characteristics resulted in a slightly lesser amount of DOX being released at pH 6.0.[58] However, at pH 7.4, the carboxylic acid groups on the SA/CMC polymeric chains became ionized, resulting in higher osmotic pressure and greater electrostatic repulsion between charged groups. As a result, SA/CMC polymeric microgels had a higher degree of swelling, leading to a higher rate of drug release. On the other hand, the rate of drug release from SACMC-DOX-NPs was lower at pH 7.4 than at 6.0. This is due to imine bond formation between the C=O group of DOX and the –NH$_2$ group of AZnFe-NPs. At pH 7.4, the bond is not completely cleaved, leading to a lower rate of drug release; whereas, at pH 6.0, the imine bond cleaves, leading to a higher rate of drug release.[59] In addition, the incorporation of AZnFe-NPs significantly retarded the release of DOX from the microgels. The presence of AZnFe-NPs in the microgels resulted in a longer distance for DOX molecules to diffuse from the microgels into the release medium, lengthening the time of drug release. In our previous study,[9] the rate of drug release from magnetite nanoparticles embedded in DOX-loaded microgels was found to be higher at pH 7.4. In the current study, the release rate was lower at pH 7.4 and higher at pH 6.0 due to imine bond formation between DOX and NPs. The developed microgels, therefore, are worth further development for use in chemotherapy to release DOX in the tumor environment.

The release kinetics of SACMC-DOX and SACMC-DOX-AZnFe-NPs were analyzed by fitting the release data into different kinetic models and the Korsmeyer-Peppas equation. Based on the r^2 values (Table 1) of the samples, drug release from SACMC-DOX and SACMC-DOX-AZnFe-NPs was found to better follow the first order model and the Higuchi model, respectively. The release mechanisms of SACMC-DOX and SACMC-DOX-AZnFe-NPs were determined based on the n values of Korsmeyer-Peppa's equation. The n values were in the range of 0.437–0.574, suggesting that drug release from both SACMC-DOX and SACMC-DOX-AZnFe-NPs was mediated largely via non-Fickian diffusion.

In Vitro Toxicity

The in vitro toxicity of SACMC-DOX, SACMC-AZnFe-NPs, and SACMC-DOX-AZnFe-NPs were examined in MCF-7 cells (Figure 6). SACMC-DOX, SACMC-AZnFe-NPs, and SACMC-DOX-AZnFe-NPs appeared to show different levels of cytotoxicity. Upon exposure to DOX, SACMC-DOX, SACMC-AZnFe-NPs, and SACMC-DOX-AZnFe-NPs, the viability of MCF-7 cells dropped to 4, 24, 38, and 16%, respectively. This suggested that upon being loaded into the microgels, the cytotoxicity of the drug was lower than that of pure DOX. This is because the microgels released DOX steadily. This result is consistent with prior research which has reported that the toxicity of the drug will be reduced when the drug is released slowly over time. Furthermore, due to the capacity of the NPs in reactive oxygen species (ROS) production as previously reported,[1] the NPs showed certain extent of cytotoxicity even in the absence of loaded DOX

Table 1 Release Kinetics Parameters of SACMC-DOX and SACMC-DOX-AZnFe-NPs in PBS of pH 7.4 and 6.0 at 37 °C

Sample	pH	Zero Order		First order		Higuchi		Korsmeyer-Peppas	
		K_0	r^2	K_l	r^2	K_H	r^2	n	r^2
SACMC-DOX	7.4	0.092	0.149	0.030	0.953	2.983	0.862	0.505	0.994
	6.0	0.083	0.372	0.020	0.939	2.665	0.914	0.570	0.993
SACMC-DOX-AZnFe-NPs	7.4	0.030	0.276	0.030	0.464	0.957	0.927	0.437	0.992
	6.0	0.077	0.373	0.020	0.901	2.473	0.915	0.574	0.996
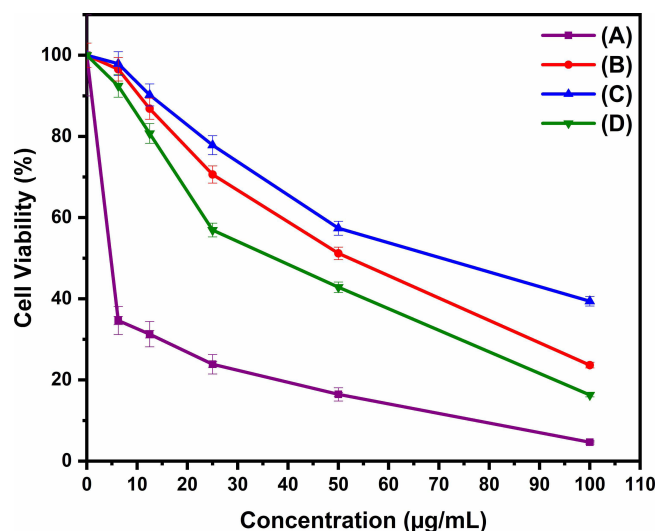
Figure 6 Cell viability of MCF-7 cells at different concentrations of (**A**) DOX, (**B**) SACMC-DOX, (**C**) SACMC-AZnFe-NPs, and (**D**) SACMC-DOX-AZnFe-NPs (n = 3). Data are shown as mean ± SD.

molecules. If this property is further exploited in development of cancer treatment, it may enhance the therapeutic effect of the delivered anti-cancer drug.

Conclusions

Development of smart composite microgels for controlled release of bioactive molecules is of great importance. In this study, pH-responsive polymeric composite microgels were created using DOX-conjugated amine-functionalized zinc ferrite NPs, SA, and CMC. FTIR analysis confirmed the interaction of AZnFe-NPs with DOX and the formation of the imine bond. It also confirmed the encapsulation of DOX in the SA/CMC polymeric matrix. XRD analyses provided additional confirmation of the generation of AZnFe-NPs and revealed the dispersion of DOX in the polymeric matrix. The generated composite microgels were found to be spherical in shape, with the size of the AZnFe-NPs being estimated to be 120–150 nm. The microgels showed good swelling capacity at both pH 6.0 and 7.4. While SACMC-DOX exhibited a higher rate of drug release at pH 7.4 than at pH 6.0, SACMC-DOX-AZnFe-NPs showed the opposite trend. The latter was attributed to the fact that the imine bond is intact at neutral pH but is cleaved under an acidic environment. Taking the stimuli-responsive properties and drug delivery performance of our microgels into account, our microgels warrant further study as a carrier for treatment development and subsequent clinical translation.

Data Sharing Statement

All data generated or analysed during this study are included in this published article.

Author Contributions

All authors made a significant contribution to the work reported, whether that is in the conception, study design, execution, acquisition of data, analysis and interpretation, or in all these areas; took part in drafting, revising or critically reviewing the article; gave final approval of the version to be published; have agreed on the journal to which the article has been submitted; and agree to be accountable for all aspects of the work.

Funding

Disclosure

The authors declare no conflict of interest.

References

1. Adilakshmi B, Reddy OS, Hemalatha D, Krishna Rao KSV, Lai W-F. ROS-generating poly (Ethylene Glycol)-Conjugated Fe3O4 nanoparticles as cancer-targeting sustained release carrier of doxorubicin. *Int J Nanomed*. 2022;Volume 17:4989–5000. doi:10.2147/IJN.S379200

2. Boddu A, Reddy OS, Zhang D, Rao KK, Lai W-F. ROS-generating, pH-responsive and highly tunable reduced graphene oxide-embedded microbeads showing intrinsic anticancer properties and multi-drug co-delivery capacity for combination cancer therapy. *Drug Deliv*. 2022;29(1):2481–2490. doi:10.1080/10717544.2022.2100512

3. Pourmadadi M, Ghohrodi AR, Savari Z, et al. Enhancing cancer therapy: the potential of mercaptopurine-based nanomaterials for targeted drug delivery. *Next Nanotechnol*. 2023;2:100018.

4. Pramanik A, Xu Z, Shamsuddin SH, et al. Affimer tagged cubosomes: targeting of carcinoembryonic antigen expressing colorectal cancer cells using in vitro and in vivo models. *ACS Appl Mater Interfaces*. 2022;14(9):11078–11091.

5. Dang Y, Guan J. Nanoparticle-based drug delivery systems for cancer therapy. *Smart Mater Med*. 2020;1:10–19. doi:10.1016/j.smaim.2020.04.001

6. Lai WF, Tang R, Wong WT. Ionically crosslinked complex gels loaded with oleic acid-containing vesicles for transdermal drug delivery. *Pharmaceutics*. 2020;12(8):725. doi:10.3390/pharmaceutics12080725

7. Lai WF, He ZD. Design and fabrication of hydrogel-based nanoparticulate systems for in vivo drug delivery. *J Control Release*. 2016;243:269–282. doi:10.1016/j.jconrel.2016.10.013

8. Pourmadadi M, Eshaghi MM, Shaghaghi M, et al. Nano-scale drug delivery systems for carboplatin: a comprehensive review. *OpenNano*. 2023;13:100175. doi:10.1016/j.onano.2023.100175

9. Obireddy SR, Chintha M, Kashayi CR, Venkata KR, Subbarao SMC. Gelatin-coated dual cross-linked sodium alginate/magnetite nanoparticle microbeads for controlled release of doxorubicin. *ChemistrySelect*. 2020;5(33):10276–10284. doi:10.1002/slct.202002604

10. J-J X, Zhang W-C, Guo Y-W, Chen X-Y, Zhang Y-N. Metal nanoparticles as a promising technology in targeted cancer treatment. *Drug Deliv*. 2022;29(1):664–678. doi:10.1080/10717544.2022.2039804

11. Anjum S, Hashim M, Malik SA, et al. Recent advances in zinc oxide nanoparticles (ZnO NPs) for cancer diagnosis, target drug delivery, and treatment. *Cancers*. 2021;13(18):4570. doi:10.3390/cancers13184570

12. Rasmussen JW, Martinez E, Louka P, Wingett DG. Zinc oxide nanoparticles for selective destruction of tumor cells and potential for drug delivery applications. *Expert Opin Drug Deliv*. 2010;7(9):1063–1077. doi:10.1517/17425247.2010.502560

13. Xiong H-M. ZnO nanoparticles applied to bioimaging and drug delivery. *Adv Mater*. 2013;25(37):5329–5335. doi:10.1002/adma.201301732

14. Kim S, Lee SY, Cho H-J. Doxorubicin-wrapped zinc oxide nanoclusters for the therapy of colorectal adenocarcinoma. *Nanomaterials*. 2017;7(11):354. doi:10.3390/nano7110354

15. Zhang Z-Y, Xiong H-M. Photoluminescent ZnO nanoparticles and their biological applications. *Materials*. 2015;8(6):3101–3127. doi:10.3390/ma8063101

16. Mishra PK, Mishra H, Ekielski A, Talegaonkar S, Vaidya B. Zinc oxide nanoparticles: a promising nanomaterial for biomedical applications. *Drug Discov Today*. 2017;22(12):1825–1834. doi:10.1016/j.drudis.2017.08.006

17. Perera WPTD, Dissanayake RK, Ranatunga UI, et al. Curcumin loaded zinc oxide nanoparticles for activity-enhanced antibacterial and anticancer applications. *RSC Adv*. 2020;10(51):30785–30795. doi:10.1039/D0RA05755J

18. Gholamali I. Stimuli-responsive polysaccharide hydrogels for biomedical applications: a review. *Regen Eng Transl Med*. 2021;7(1):91–114. doi:10.1007/s40883-019-00134-1

19. Yadollahi M, Farhoudian S, Barkhordari S, Gholamali I, Farhadnejad H, Motasadizadeh H. Facile synthesis of chitosan/ZnO bio-nanocomposite hydrogel beads as drug delivery systems. *Int J Biol Macromol*. 2016;82:273–278. doi:10.1016/j.ijbiomac.2015.09.064

20. Gholamali I, Yadollahi M. Doxorubicin-loaded carboxymethyl cellulose/Starch/ZnO nanocomposite hydrogel beads as an anticancer drug carrier agent. *Int J Biol Macromol*. 2020;160:724–735. doi:10.1016/j.ijbiomac.2020.05.232

21. Lai W-F, Huang EM, Wong W-T. A gel-forming clusteroluminogenic polymer with tunable emission behavior as a sustained-release carrier enabling real-time tracking during bioactive agent delivery. *Appl Mater Today*. 2020;21:100876. doi:10.1016/j.apmt.2020.100876

22. Wu T, Huang J, Jiang Y, et al. Formation of hydrogels based on chitosan/alginate for the delivery of lysozyme and their antibacterial activity. *Food Chem*. 2018;240:361–369. doi:10.1016/j.foodchem.2017.07.052

23. Sanchez-Ballester NM, Soulairol I, Bataille B, Sharkawi T. Flexible heteroionic calcium-magnesium alginate beads for controlled drug release. *Carbohydr Polym*. 2019;207:224–229. doi:10.1016/j.carbpol.2018.11.096

24. Sreekanth Reddy O, Subha MCS, Jithendra T, Madhavi C, Chowdoji Rao K. Curcumin encapsulated dual cross linked sodium alginate/montmorillonite polymeric composite beads for controlled drug delivery. *J Pharm Anal*. 2021;11(2):191–199. doi:10.1016/j.jpha.2020.07.002

25. Leonel AG, Mansur HS, Mansur AAP, et al. Synthesis and characterization of iron oxide nanoparticles/carboxymethyl cellulose core-shell nanohybrids for killing cancer cells in vitro. *Int J Biol Macromol*. 2019;132:677–691. doi:10.1016/j.ijbiomac.2019.04.006

26. Zare-Akbari Z, Farhadnejad H, Furughi-Nia B, Abedin S, Yadollahi M, Khorsand-Ghayeni M. PH-sensitive bionanocomposite hydrogel beads based on carboxymethyl cellulose/ZnO nanoparticle as drug carrier. *Int J Biol Macromol*. 2016;93:1317–1327. doi:10.1016/j.ijbiomac.2016.09.110

27. Lai W-F, Shum HC. A stimuli-responsive nanoparticulate system using poly(ethylenimine)-graft-polysorbate for controlled protein release. *Nanoscale*. 2016;8(1):517–528. doi:10.1039/C5NR06641G

28. Lai W-F, Susha AS, Rogach AL. Multicompartment microgel beads for co-delivery of multiple drugs at individual release rates. *ACS Appl Mater Interfaces*. 2016;8(1):871–880. doi:10.1021/acsami.5b10274

29. Lai WF, Deng R, He T, Wong WT. A bioinspired, sustained-release material in response to internal signals for biphasic chemical sensing in wound therapy. *Adv Healthc Mater*. 2021;10(2):e2001267. doi:10.1002/adhm.202001267

30. Bashir S, Hina M, Iqbal J, et al. Fundamental concepts of hydrogels: synthesis, properties, and their applications. *Polymers*. 2020;12(11):2702. doi:10.3390/polym12112702

31. Jiang Y, Krishnan N, Heo J, Fang RH, Zhang L. Nanoparticle–hydrogel superstructures for biomedical applications. *J Control Release*. 2020;324:505–521.

32. Gaharwar AK, Peppas NA, Khademhosseini A. Nanocomposite hydrogels for biomedical applications. *Biotechnol Bioeng*. 2014;111(3):441–453. doi:10.1002/bit.25160

33. Mahmood RI, Kadhim AA, Ibraheem S, et al. Biosynthesis of copper oxide nanoparticles mediated Annona muricata as cytotoxic and apoptosis inducer factor in breast cancer cell lines. *Sci Rep*. 2022;12(1):16165. doi:10.1038/s41598-022-20360-y

34. Stepankova H, Swiatkowski M, Kruszynski R, et al. The anti-proliferative activity of coordination compound-based ZnO nanoparticles as a promising agent against triple negative breast cancer cells. *Int J Nanomed*. 2021;16:4431. doi:10.2147/IJN.S304902

35. Obireddy SR, Lai W-F. ROS-generating amine-functionalized magnetic nanoparticles coupled with carboxymethyl chitosan for pH-responsive release of doxorubicin. *Int J Nanomed*. 2022;17:589–601. doi:10.2147/IJN.S338897

36. Farhoudian S, Yadollahi M, Namazi H. Facile synthesis of antibacterial chitosan/CuO bio-nanocomposite hydrogel beads. *Int J Biol Macromol*. 2016;82:837–843. doi:10.1016/j.ijbiomac.2015.10.018

37. Yadollahi M, Farhoudian S, Namazi H. One-pot synthesis of antibacterial chitosan/silver bio-nanocomposite hydrogel beads as drug delivery systems. *Int J Biol Macromol*. 2015;79:37–43. doi:10.1016/j.ijbiomac.2015.04.032

38. Giri TK. 20 - Alginate Containing Nanoarchitectonics for Improved Cancer Therapy. In: Holban AM, Grumezescu AM, editors. *Nanoarchitectonics for Smart Delivery and Drug Targeting*. William Andrew Publishing; 2016:565–588.

39. Pedroso-Santana S, Fleitas-Salazar N. Ionotropic gelation method in the synthesis of nanoparticles/microparticles for biomedical purposes. *Polym Int*. 2020;69(5):443–447. doi:10.1002/pi.5970

40. Sacco P, Pedroso-Santana S, Kumar Y, Joly N, Martin P, Bocchetta P. Ionotropic gelation of chitosan flat structures and potential applications. *Molecules*. 2021;26(3):660. doi:10.3390/molecules26030660

41. Cánepa C, Imperiale JC, Berini CA, Lewicki M, Sosnik A, Biglione MM. Development of a drug delivery system based on chitosan nanoparticles for oral administration of interferon-α. *Biomacromolecules*. 2017;18(10):3302–3309. doi:10.1021/acs.biomac.7b00059

42. Reddy NS, Eswaramma S, Chung I, Rao KK, Ramesh P, Chandra Sekhar A. Chitosan/poly(dimethylaminoethylmethacrylate-co-hydroxyethylacrylate) based semi-IPN hydrogels and silver nanocomposites: synthesis, evaluation of amoxicillin release studies, and antibacterial studies. *Int J Polym Mater Polym Biomater*. 2019;68(14):870–880. doi:10.1080/00914037.2018.1517349

43. Lai WF, Susha AS, Rogach AL, et al. Electrospray-mediated preparation of compositionally homogeneous core–shell hydrogel microspheres for sustained drug release. *RSC Adv*. 2017;7:44482–44491. doi:10.1039/C7RA07568E

44. Pallerla D, Banoth S, Jyothi S. Fabrication of nano clay intercalated polymeric microbeads for controlled release of curcumin. *Int J Appl Pharm*. 2021;13(1):206–215. doi:10.22159/ijap.2021v13i1.39965

45. Jithendra T, Reddy OS, Subha MCS, Rao KC. Fabrication of drug delivery system for controlled release of curcumin, intercalated with magnetite nanoparticles through sodium alginate/polyvinylpyrrolidone-co-vinyl acetate semi-IPN microbeads. *Int J Appl Pharm*. 2020;12:249–257. doi:10.22159/ijap.2020v12i5.37761

46. Chintha M, Obireddy SR, Areti P, Marata Chinna Subbarao S, Kashayi CR, Rapoli JK. Sodium alginate/locust bean gum-g-methacrylic acid IPN hydrogels for "simvastatin" drug delivery. *J Dispers Sci Technol*. 2020;41(14):2192–2202. doi:10.1080/01932691.2019.1677247

47. Costa P, Sousa Lobo JM. Modeling and comparison of dissolution profiles. *Eur J Pharm Sci*. 2001;13(2):123–133.

48. Rao KM, Kumar A, Suneetha M, Han SS. pH and near-infrared active; chitosan-coated halloysite nanotubes loaded with curcumin-Au hybrid nanoparticles for cancer drug delivery. *Int J Biol Macromol*. 2018;112:119–125. doi:10.1016/j.ijbiomac.2018.01.163

49. Matloubi Moghaddam F, Doulabi M, Saeidian H. Controlled microwave-assisted synthesis of ZnFe2O4 nanoparticles and their catalytic activity for O-acylation of alcohol and phenol in acetic anhydride. *Sci Iran*. 2012;19(6):1597–1600. doi:10.1016/j.scient.2012.10.013

50. Lungu II, Nistorescu S, Badea MA, et al. Doxorubicin-conjugated iron oxide nanoparticles synthesized by laser pyrolysis: in vitro study on human breast cancer cells. *Polymers*. 2020;12(12):2799. doi:10.3390/polym12122799

51. Zhang X, Chen Z, Liu J, Cui S. Synthesis and characterization of ZnFe2O4 nanoparticles on infrared radiation by xerogel with sol-gel method. *Chem Phys Lett*. 2021;764:138265. doi:10.1016/j.cplett.2020.138265

52. Lanz-Landázuri A, Martínez de Ilarduya A, García-Alvarez M, Muñoz-Guerra S. Poly(β,L-malic acid)/Doxorubicin ionic complex: a pH-dependent delivery system. *React Funct Polym*. 2014;81:45–53. doi:10.1016/j.reactfunctpolym.2014.04.005

53. Li L, Fan H, Wang L, Jin Z. Does halloysite behave like an inert carrier for doxorubicin? *RSC Adv*. 2016;6(59):54193–54201.

54. Reddy OS, Subha MCS, Jithendra T, Madhavi C, Rao KC. Fabrication and characterization of smart karaya gum/sodium alginate semi-IPN microbeads for controlled release of D-penicillamine drug. *Polym Polym Compos*. 2020;29(3):163–175.

55. Padma GT, Rao TS, Naidu KCB. Preparation, characterization and dielectric properties of sodium alginate/titanium dioxide composite membranes. *SN Appl Sci*. 2018;1(1):75. doi:10.1007/s42452-018-0083-y

56. Pourmadadi M, Rahmani E, Shamsabadipour A, et al. Role of Iron Oxide (Fe2O3) Nanocomposites in advanced biomedical applications: a state-of-the-art review. *Nanomaterials*. 2022;12(21):3873.

57. Akl MA, Kamel AM, El-Ghaffar MAA. Biodegradable functionalized magnetite nanoparticles as binary-targeting carrier for breast carcinoma. *BMC Chem*. 2023;17(1):3. doi:10.1186/s13065-023-00915-4

58. Eswaramma S, Rao KK. Synthesis of dual responsive carbohydrate polymer based IPN microbeads for controlled release of anti-HIV drug. *Carbohydr Polym*. 2017;156:125–134. doi:10.1016/j.carbpol.2016.09.023

59. Tao Y, Liu S, Zhang Y, Chi Z, Xu J. A pH-responsive polymer based on dynamic imine bonds as a drug delivery material with pseudo target release behavior. *Polym Chem*. 2018;9(7):878–884. doi:10.1039/C7PY02108A